ARCHIVES OF ELECTRICAL ENGINEERING VOL. 65(4), pp. 719-732 (2016)

DOI 10.1515/aee-2016-0050

Modeling of linear dispersive materials using scalable time domain finite element scheme

BOGUSŁAW BUTRYŁO

Faculty of Electrical Engineering, Bialystok University of Technology
ul. Wiejska 45d, 15-351 Białystok, Poland
e-mail: b.butrylo@pb.edu.pl

(Received: 17.12.2015, revised: 12.09.2016)

Abstract: This paper deals with some aspects of formulation and implementation of a broadband algorithm with build-in analysis of some dispersive media. The construction of the finite element method (FEM) based on direct integration of Maxwell's equations and solution of some additional convolution integrals is presented. The broadband, fractional model of permittivity is approximated by a set of some relaxation sub-models. The properties of the 3D time-dependent formulation of the FEM algorithm are determined using a benchmark problem with the Cole-Cole and the Davidson-Cole models. Several issues associated with the implementation and some constraints of the broadband finite element algorithm are presented.

Key words: dispersive dielectrics, electromagnetic field, finite element method, fractional relaxation, wideband numerical scheme

1. Introduction

The development of high frequency and microwave components is driven by many factors, but recently material technologies have played a leading part. Instead of conventional materials, there are a growing number of attempts to implement composites. The right choice of constituents and some modifications of the microscopic structure enable to shape the electric properties of materials. Much recent effort has been devoted to developing some smart, frequency selective materials. Their properties can be shaped using some dispersive materials [1, 2].

A qualitative analysis and a reliable designing of the components containing materials exhibiting electrical dispersion can be performed using some numerical methods [3]. To simulate wideband electromagnetic phenomena, the frequency dependencies of permittivity have to be reflected in the implemented algorithm. Consequently, the set of constraints and the number of factors that determine the structure and properties of the algorithm have enlarged.

This paper takes a look at the formulation and properties of a wideband finite element (FE) algorithm with direct integration of Maxwell's equations in time domain. The main issues related to numerical modeling of dispersive materials with the complex profiles of permittivity are presented. Some aspects connected with the structure of the developed finite-element time-domain (FETD) algorithm are characterized. The algorithm is validated by considering a benchmark problem, with a dielectric plate illuminated by the wideband electromagnetic pulse. The computational tests are performed assuming different models of fractional relaxation. Finally, some concluding remarks related to scalability and flexibility, as well as some constraints of the FETD algorithm are given.

2. Model of dielectric relaxation

Assuming linear properties of a material, the constitutive relation between the vector of electric displacement $\vec{\boldsymbol{D}}$ and the vector of electric field intensity $\vec{\boldsymbol{E}}$ takes a form of a complex function defined in a selected frequency band $f \in \langle f_{\min}, f_{\max} \rangle$

$$\underline{\vec{\boldsymbol{D}}}(f) = \varepsilon_0 \underline{\varepsilon}_{r,\mathrm{eff}}(f)\, \underline{\vec{\boldsymbol{E}}}(f), \tag{1}$$

where ε_0 is the vacuum permittivity, $\underline{\varepsilon}_{r,\mathrm{eff}}(f)$ is the relative, effective permittivity of material. In a typical, narrowband approach, the problem comes down to a single point of the permittivity function $\underline{\varepsilon}_{r,\mathrm{eff}}(f) \equiv \underline{\varepsilon}_{r,\mathrm{eff}}(f_1)$, where f_1 is the frequency of the propagated wave. Analysis of a problem with a non-harmonic electromagnetic waveform enforces transition to the wideband definition of the model. The macroscopic properties of the dispersive material can be expressed as an empirical function [4, 5]

$$\underline{\varepsilon}_{r,eff}(f) = \varepsilon_\infty + \underline{\chi}(f) = \varepsilon_\infty + \sum_{k=1}^{N_\chi} \underline{\chi}_k(f), \tag{2}$$

where ε_∞ is the infinite frequency permittivity, and $\underline{\chi}(f)$ is the electric susceptibility function. The formulated model is a linear combination of some selected sub-models, where the number of components is stated by N_χ. Some real, single-pole components concern the relaxation dispersion, while some complex-conjugate pole-residue pairs describe the resonance phenomena [5]. The wideband formulation of the algorithm with build in analysis of the resonance dispersion was presented in [6]. In this report we concentrate on some empirical, fractional relaxation models.

In a general form, the k-th component of the susceptibility function can be expressed by the fractional, Havriliak-Negami model [5]

$$\underline{\chi}_k(f) = \frac{\Delta_{\varepsilon,k}}{\left(1 + (j\omega\tau_{0,k})^{\alpha_k}\right)^{\beta_k}}, \tag{3}$$

where $\Delta_{\varepsilon,k}$ denotes the relative permittivity decrement, and $\tau_{0,k}$ is the relaxation time. The form of the sub-model is fitted to the real dispersity profile by modification of the deformation coefficients $\alpha_k \in \langle 0, 1\rangle$ and $\beta_k \in \langle 0, 1\rangle$. The fractional relaxation models can be mapped in the coordinate system $\{\alpha, \beta, \tau_0\}$ (Fig. 1a). The Havriliak-Negami model (χ_{HN}: $\alpha_k < 1$, $\beta_k < 1$) covers some other variants of relaxation, i.e. the Cole-Cole model (χ_{CC}: $\alpha_k < 1$, $\beta_k = 1$), and the Davidson-Cole model (χ_{DC}: $\alpha_k = 1$, $\beta_k < 1$). The Debye model (χ_D: $\alpha_k = 1$, $\beta_k = 1$) corresponds to the ideal case, when the material consists of particles having the same properties. Direct numerical implementation of the Havriliak-Negami formula is unfeasible. Transferring the function (3) into a time domain yields an infinite functional series, where the independent variable t is in a fractional power.

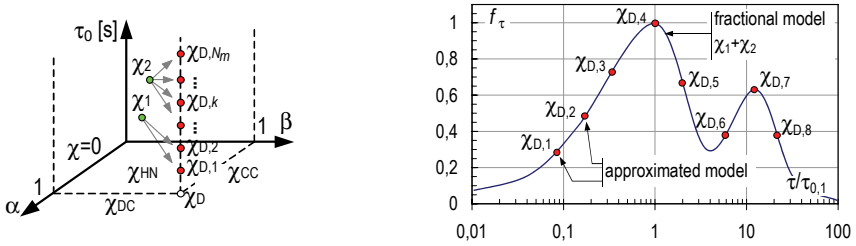

(a) (b)

Fig. 1. Mapping of the fractional relaxation model into a set of Debye models (a), an example of the normalized relaxation time distribution function f_τ and some components of the approximated model (b)

The fractional models can be characterized by a distribution of relaxation times $f_\tau = f(\tau_0)$ [5]. The deformation coefficients α_k and β_k determine the form of the function f_τ. According to the Schweidler paradigm, the broader dispersion of the complex materials can be described in terms of the superposition of Debye-like relaxation processes. In this approach the complex dispersity of the material is projected to the set of the ordinary sub-models (Fig. 1a). The continuous relaxation time distribution function f_τ is sampled (Fig. 1b), and the complex model is reduced to a set of points [7]. To improve the quality of approximation we should consider some components described by different dynamics ($\tau < \tau_{0,k}$ and $\tau > \tau_{0,k}$). The components of the constructed model are Fourier transformed

$$\underline{\chi}(f) \cong \sum_{k=1}^{N_m} \underline{\chi}_{D,k}(f) \quad \rightarrow \quad \chi(t) = \sum_{k=1}^{N_m} \frac{\Delta_{\varepsilon,k}}{\tau_k} e^{-t/\tau_k} \mathbf{1}(t), \tag{4}$$

where $\mathbf{1}(t)$ is the unit step function, and N_m is the total number of poles in the approximated model.

3. Formulation of the algorithm

Since the electric permittivity can be changed in a predefined frequency spectrum, a reliable estimation of electromagnetic field can be obtained using a full-wave time-domain for-

mulation [8]. The governing vector wave equation is derived from Maxwell's equations for some linear and isotropic media [6, 9]

$$\nabla\times\frac{1}{\mu_0\mu_r}\nabla\times\vec{\boldsymbol{E}}+\sigma\frac{\partial\vec{\boldsymbol{E}}}{\partial t}+\frac{\partial^2\vec{\boldsymbol{D}}}{\partial t^2}=0\,, \tag{5}$$

where μ_r is the relative permeability, and σ is the static electric conductivity. The electric flux vector $\vec{\boldsymbol{D}}$ implicitly expresses dispersion of material. Substitution of (2) into (1) and the Fourier inverse of this expression yield the time domain representation of the electric displacement vector. Assuming zero values of the electric field intensity $\vec{\boldsymbol{E}}$ and the kernel susceptibility function $\chi_{D,k}(t)$ for negative time, the instantaneous value of the flux density is governed by equation

$$\vec{\boldsymbol{D}}(t)=\varepsilon_0\varepsilon_\infty\,\vec{\boldsymbol{E}}(t)+\varepsilon_0\sum_{k=1}^{\mathbf{N_m}}\int_0^t\chi_{\mathrm{D},\mathbf{k}}(t-\eta)\,\vec{\boldsymbol{E}}(\eta)d\eta=\varepsilon_0\varepsilon_\infty\,\vec{\boldsymbol{E}}(t)+\varepsilon_0\sum_{k=1}^{\mathbf{N_m}}\vec{\mathbf{C}}_k(t), \tag{6}$$

where $\vec{\boldsymbol{C}}_k(t)$ is the instantaneous value of the convolution integral, related to the k-th sub-model ($\chi_{D,k}$). According to Eqs. (5) and (6), the wideband model can be split into the fundamental part and the supplementary one (Fig. 2).

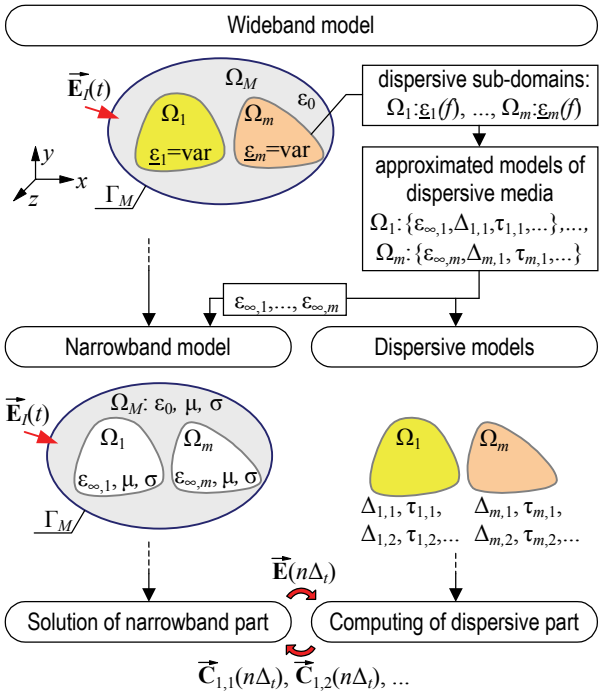

Fig. 2. The diagram of the broadband finite element algorithm

The fundamental part (shortly called the narrowband model) is connected with calculation of electric field distribution. It is defined in the whole volume Ω_M. The supplementary part

(called the dispersive model) is related to dispersive materials. This model is constructed only in the regions where the material susceptibility is not constant, $\Omega_M \subset \{\Omega_1, ..., \Omega_m\}$. The number of created sub-models is equal to the total number of poles N_m.

In the final form of the algorithm the instantaneous distributions of the vector quantities are determined as a result of an iterative scheme. The numerical integration of the discrete forms of Eqs. (5) and (6) is interlaced. The instantaneous values of the field intensity $\vec{\boldsymbol{E}}$ and the flux density $\vec{\boldsymbol{D}}$ vectors must be passed between these routines. The narrowband part and the supplementary one are synchronized, but the specific numerical methods can be independently selected. Two general constraints should be taken into consideration in the structure of the developed algorithm.

- The components of the electric field vector and the electric displacement vector should be defined in the same points of the volume Ω_M.
- Computations of the instantaneous values of the electric intensity and the convolutions are carried out with the same time step Δ_t.

The finite difference algorithm with direct integration of the constitutive equations in time domain (FDTD, finite-difference time-domain) is the most popular approach to analyse the dispersive problems [10-12]. The reported work is concentrate on the development of the broadband finite element algorithm [13, 14], based on the edge elements $H(rot, \Omega_M)$ [15]. For discretizing Eq. (5), the volume of the model Ω_M is meshed with the tetrahedral $H(rot, \Omega_M)$ elements. This class of elements seems to be adequate basis to approximate the vector fields. The degrees of freedom are the voltages $u_j(t)$ (j = 1, 2, …, N_{DOF}) defined along the edges of the FE mesh. There is one vector test function $\vec{w}_j$ for every edge in the mesh. The local, time dependent distribution of the field in the e-th element is stated by equation

$$\vec{\boldsymbol{E}}_e(t) = \sum_{j=1}^{N_e} u_j(t)\vec{\boldsymbol{w}}_j = \sum_{j=1}^{N_e} E_{t,j}(t) l_j \vec{\boldsymbol{w}}_j \,, \tag{7}$$

where $E_{t,j}(t)$ is the tangential component of the electric field intensity defined along the j-th edge, l_j is the length of the edge, and N_e is the number of edges in the element. The edge elements enforce the tangential continuity of the field across the boundary, while the normal components of the field are free. It is a fundamental condition when dealing with dielectrics. In this way, the implementation of the essential boundary conditions is much easier than in the typical nodal formulation of the FE method. Since the time-dependent value of the $E_{t,j}(t)$ is defined locally, the $H(rot, \Omega_M)$ elements correctly approximate propagation of the wideband electromagnetic waveforms through dispersive dielectrics.

The resulting Galerk in form of (5) is given by

$$\begin{aligned} &\int_{\Omega_e} \frac{1}{\mu_0 \mu_r} \left(\nabla \times \vec{\boldsymbol{w}}_i\right) \cdot \left(\nabla \times \vec{\boldsymbol{E}}_e\right) \mathrm{d}\Omega + \int_{\Omega_e} \sigma \vec{\boldsymbol{w}}_i \cdot \frac{\partial \vec{\boldsymbol{E}}_e}{\partial t} \mathrm{d}\Omega + \\ &+ \int_{\Omega_e} \varepsilon_0 \varepsilon_\infty \vec{\boldsymbol{w}}_i \cdot \frac{\partial^2 \vec{\boldsymbol{E}}_e}{\partial t^2} \mathrm{d}\Omega + \sum_{k=1}^{N_m} \int_{\Omega_e} \varepsilon_0 \vec{\boldsymbol{w}}_i \cdot \frac{\partial^2 \vec{\boldsymbol{C}}_k}{\partial t^2} \mathrm{d}\Omega = 0, \end{aligned} \tag{8}$$

where Ω_e denotes the volume of the e-th element of the mesh, and $\vec{w}_j$ is the vector test function ($i = 1, ..., N_{\mathrm{DOF}}$). Assembling of Equation (8) over the edges in the FE mesh leads to formulation of the matrix equation. The calculation of the electric field in the narrowband model (Fig. 2) comes down to a solution of the ordinary differential equation

$$\boldsymbol{T}\frac{\mathrm{d}^2\boldsymbol{e}}{\mathrm{d}t^2}+\sum_{m=1}^{N}\left(\sum_{k=1}^{N_m}\boldsymbol{U}\frac{\mathrm{d}^2}{\mathrm{d}t^2}\boldsymbol{c}_k\right)+\boldsymbol{R}\frac{\mathrm{d}\boldsymbol{e}}{\mathrm{d}t}+\boldsymbol{S}\cdot\boldsymbol{e}=0\,, \tag{9}$$

where the vector $\boldsymbol{e}$ consists of the $E_{t,j}$ coefficients ($\dim \boldsymbol{e} = N_{\mathrm{DOF}}$). The respective matrix components are determined using formulas

$$t_{ij}=\int_{\Omega_e}\varepsilon_0\varepsilon_\infty\vec{\boldsymbol{w}}_i\cdot\vec{\boldsymbol{w}}_j\mathrm{d}\Omega\,, \tag{10a}$$

$$u_{ij}=\int_{\Omega_e}\varepsilon_0\vec{\boldsymbol{w}}_i\cdot\vec{\boldsymbol{w}}_j\mathrm{d}\Omega\,, \tag{10b}$$

$$r_{ij}=\int_{\Omega_e}\sigma\vec{\boldsymbol{w}}_i\cdot\vec{\boldsymbol{w}}_j\mathrm{d}\Omega\,, \tag{10c}$$

$$s_{ij}=\int_{\Omega_e}\frac{1}{\mu}\left(\nabla\times\vec{\boldsymbol{w}}_i\right)\cdot\left(\nabla\times\vec{\boldsymbol{w}}_j\right)\mathrm{d}\Omega\,. \tag{10d}$$

The values of coefficients t_{ij}, u_{ij}, r_{ij}, s_{ij} remain fixed, because they depend on the material parameters valid for the narrowband part. According to the Eqs. (9) and (10), the nature of the polarization phenomena and the parameters of the poles $\chi_{\mathrm{D},k}$ do not have a direct impact on the components of the matrices.

Discretization of the time derivatives in (9) enables to calculate the instantaneous values of the electric field intensity $\boldsymbol{e}(t) \equiv \boldsymbol{e}(n\Delta_t)=\boldsymbol{e}_n$. The order of the constructed scheme can be modified by selecting appropriate approximations of the derivatives. We can implement either conditionally or unconditionally stable time integration scheme. In this formulation the time stepping solution is attained through the second order, unconditionally stable Newmark-Beta scheme [14]. The resulting update equation is

$$\begin{aligned}&\left(\boldsymbol{T}_\infty+\frac{\Delta_t}{2}\boldsymbol{R}+\frac{\Delta_t^2}{4}\boldsymbol{S}+\sum_{k=1}^{N_m}r_{k,1}\boldsymbol{T}_0\right)\cdot\boldsymbol{e}_{n+1}=\left(2\boldsymbol{T}_\infty-\frac{\Delta_t^2}{2}\boldsymbol{S}\right)\cdot\boldsymbol{e}_n+\\&+\left(-\boldsymbol{T}_\infty+\frac{\Delta_t}{2}\boldsymbol{R}-\frac{\Delta_t^2}{4}\boldsymbol{S}\right)\cdot\boldsymbol{e}_{n-1}+\sum_{k=1}^{N_m}\left(2-\mathrm{e}^{-\Delta_t/\tau_k}\right)\boldsymbol{T}_0\cdot\boldsymbol{c}_{k,n}-\sum_{k=1}^{N_m}\boldsymbol{T}_0\cdot\boldsymbol{c}_{k,n-1},\end{aligned} \tag{11}$$

where $\boldsymbol{c}_{k,n}$ is the instantaneous value of the convolution integral in the n-th time step, related to the k-th pole ($\chi_{\mathrm{D},k}$), and r_k is the coefficient assigned to the k-th pole. Its value depends on the

integration rule applied to compute the convolution integral in the supplementary part. The r_k is equal to the multiplier of the $\boldsymbol{e}_{n+1}$ vector in (14), (15) or (16).

The contribution of electric polarization in the analysed model is expressed by a set of convolution integrals (the second component of Eq. (6)). The first component of this equation is included to the narrowband part of the algorithm, since the ε_∞ is defined locally and it remains constant. According to (4), the susceptibility kernel of any sub-model is expressed by the exponential function. This assumption leads to the definition of a discrete, recursive scheme of convolution

$$\forall_{k=1,\ldots,N_m} \boldsymbol{c}_{k,n+1} = \boldsymbol{c}_{k,n} e^{-\Delta_t/\tau_k} + \int_{\Delta_t} \chi_{\mathrm{D},k}(t)\boldsymbol{e}_\Delta(t)\mathrm{d}t, \tag{12}$$

where $\boldsymbol{e}_\Delta$ is a function defined over the time interval Δ_t, which approximate local value of the electric field intensity (Fig. 3). The form of the $\boldsymbol{e}_\Delta$ is adopted in every time step

$$\boldsymbol{e}_\Delta(t) \equiv \boldsymbol{e}_\Delta(n\Delta_t) = f(\boldsymbol{e}_{n+1}, \boldsymbol{e}_n, \boldsymbol{e}_{n-1}, \boldsymbol{e}_{n-2}, \ldots) \tag{13}$$

with $t \in \langle 0, \Delta_t \rangle$, and some different approximation techniques can be used. In this approach an arbitrary computed waveform of the field intensity is expressed by polynomial. Due to the different dynamics of sub-models, the order of the polynomial can be independently matched for the successive poles of the susceptibility (4).

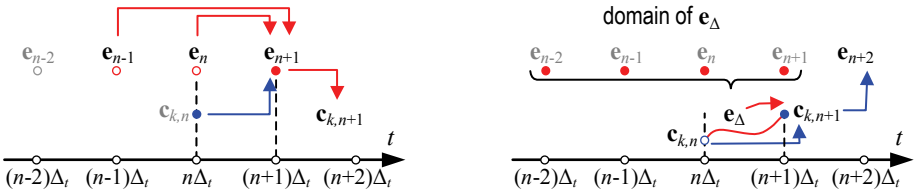

Fig. 3. Time dependencies of computed variables: the narrowband part (a), the dispersive part (b)

If $\tau_k \gg \Delta_t$, we can apply a simplified method of numerical integration, assuming constant value over the period Δ_t ($\boldsymbol{e}_\Delta$ = const = $\boldsymbol{e}_n$). In this case the relaxation time of the sub-model does not impose some critical requirements, and the constant recursive (CR) scheme is a reasonable choice. The discrete convolution integral (12) is stated by equation

$$\boldsymbol{c}_{k,n+1} = \boldsymbol{c}_{k,n} e^{-\frac{\Delta_t}{\tau_k}} + \Delta_{\varepsilon,k}\left(1 - e^{-\frac{\Delta_t}{\tau_k}}\right)\boldsymbol{e}_n. \tag{14}$$

If $\tau_k \approx \Delta_t$ we should modify the form of the $\boldsymbol{e}_\Delta$ function rather than reducing the value of the time integration step Δ_t. The value of the approximation error becomes lower when the order of implemented polynomial increases. The coefficients of the polynomial are calculated using a selected multipoint, approximation scheme, e.g. the linear approximation scheme is given by

$$\boldsymbol{c}_{k,n+1} = \boldsymbol{c}_{k,n} e^{-\frac{\Delta_t}{\tau_k}} + \frac{\Delta_{\varepsilon,k}\tau_k}{\Delta_t}\left(\frac{\Delta_t}{\tau_k} - 1 + e^{-\frac{\Delta_t}{\tau_k}}\right)\boldsymbol{e}_{n+1} + \frac{\Delta_{\varepsilon,k}\tau_k}{\Delta_t}\left(1 - \left(1 + \frac{\Delta_t}{\tau_k}\right)e^{-\frac{\Delta_t}{\tau_k}}\right)\boldsymbol{e}_n, \tag{15}$$

while the recursive parabolic approximation scheme is written as

$$\begin{aligned}\boldsymbol{c}_{k,n+1} = \boldsymbol{c}_{k,n} e^{-\frac{\Delta_t}{\tau_k}} &+ \frac{\Delta_{\varepsilon,k}\tau_k}{\Delta_t}\left(\frac{2\Delta_t^2 - 3\Delta_t\tau_k - 2\tau_k^2}{2\Delta_t\tau_k} + \frac{\Delta_t - 2\tau_k}{2\Delta_t}e^{-\frac{\Delta_t}{\tau_k}}\right)\boldsymbol{e}_{n+1} + \\ &+ \frac{\Delta_{\varepsilon,k}\tau_k}{\Delta_t}\left(2\frac{\Delta_t - \tau_k}{\Delta_t} + \frac{2\tau_k^2 - \Delta_t^2}{\Delta_t\tau_k}e^{-\frac{\Delta_t}{\tau_k}}\right)\boldsymbol{e}_n + \\ &+ \frac{\Delta_{\varepsilon,k}\tau_k}{\Delta_t}\left(\frac{\tau_k - \Delta_t}{\Delta_t} - \frac{2\tau_k - \Delta_t}{2\Delta_t}e^{-\frac{\Delta_t}{\tau_k}}\right)\boldsymbol{e}_{n-1}.\end{aligned} \tag{16}$$

4. Numerical results

In order to demonstrate the properties of this approach, a benchmark model with the dispersive media is calculated. A pulsed plane wave

$$\vec{\boldsymbol{E}}_I(t) = \left(e^{-1.5\cdot10^{10}t} - e^{-2.4\cdot10^{10}t}\right)\cdot\vec{\mathbf{1}}_x\cdot\mathbf{1}(t) \tag{17}$$

normally incidents on a plate (Fig. 4). The cut-off frequency of the pulse is $f_{I,\max} = 1.48$ GHz. The unbounded space of the discovered problem is truncated to the cuboidal domain Ω_M ($d_x = d_y = d_z = 0.4$ m). The first order Engquist-Majda absorbing boundary conditions are located at the outer surface Γ_M. The observation points are placed inside the plate (P_1) and in front of the plate (P_2).

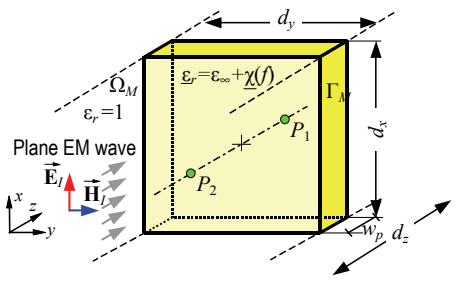

Fig. 4. Isometric view of the 3D benchmark model ($w_p = 0.2$ m)

The single pole Debye model, the Cole-Cole model, or the Davidson-Cole one expresses the relaxation properties of the illuminated body. The spectrum of the propagated electro-

magnetic wave includes frequencies where the permittivity of the material is varying. The maximum losses related with polarization of materials occur at frequencies $f_D = f_{CC} = 194.09$ MHz and $f_{DC} = 366.1$ MHz. Referring to (4), the considered fractional relaxation models are approximated by a linear combination of nine ordinary models ($N_m = 9$). The parameters of the initial and the approximated models are given in Table 1. The Cole-Cole graphs of these models are confronted in Fig. 5. The quality of approximation is validated using the Euclidean norm

$$\delta_{\chi,2} = \left\| \underline{\chi}(f) - \sum_{k=1}^{N_m} \underline{\chi}_{\mathrm{D},k}(f) \right\|_2 , \tag{18}$$

with $f \in \langle 0, 5\ \mathrm{GHz} \rangle$. The maximum value of the approximation error is 0.1248 and 0.0836 for the Cole-Cole model and the Davidson-Cole model, respectively.

Table 1. Specification of the analytical and the approximated models

	Analytical model (exact)	**Components of the approximated model**		
		symbol	$\Delta_{\varepsilon,k}$	τ_k **(s)**
Debye, $\chi \equiv \chi_D$	ε_∞=1 $\Delta_\varepsilon = 15$ $\tau_0 = 8.2\cdot10^{-10}$ (s) $\alpha = 1$ $\beta = 1$	$\chi_{D,1}$	15	$8.2\cdot10^{-10}$
Cole-Cole, $\chi \equiv \chi_{CC}$	ε_∞=1 $\Delta_\varepsilon = 15$ $\tau_0 = 8.2\cdot10^{-10}$ (s) $\alpha = 0.45$ $\beta = 1$	$\chi_{D,1}$	0.2609	$2.735\cdot10^{-13}$
		$\chi_{D,2}$	0.6321	$2.024\cdot10^{-12}$
		$\chi_{D,3}$	1.4788	$1.497\cdot10^{-11}$
		$\chi_{D,4}$	3.0388	$1.108\cdot10^{-10}$
		$\chi_{D,5}$	4.1787	$8.200\cdot10^{-10}$
		$\chi_{D,6}$	3.0388	$6.068\cdot10^{-9}$
		$\chi_{D,7}$	1.4788	$4.490\cdot10^{-8}$
		$\chi_{D,8}$	0.6321	$3.323\cdot10^{-7}$
		$\chi_{D,9}$	0.2609	$2.459\cdot10^{-6}$
Davidson-Cole, $X \equiv \chi_{DC}$	ε_∞=1 $\Delta_\varepsilon = 15$ $\tau_0 = 8.2\cdot10^{-10}$ (s) $\alpha = 1$ $\beta = 0.45$	$\chi_{D,1}$	0.0510	$3.693\cdot10^{-14}$
		$\chi_{D,2}$	0.1036	$1.238\cdot10^{-13}$
		$\chi_{D,3}$	0.1859	$4.148\cdot10^{-13}$
		$\chi_{D,4}$	0.3242	$1.390\cdot10^{-12}$
		$\chi_{D,5}$	0.5616	$4.660\cdot10^{-12}$
		$\chi_{D,6}$	0.9743	$1.562\cdot10^{-11}$
		$\chi_{D,7}$	1.7134	$5.234\cdot10^{-11}$
		$\chi_{D,8}$	3.1775	$1.754\cdot10^{-10}$
		$\chi_{D,9}$	7.9085	$5.880\cdot10^{-10}$

To demonstrate the properties of the elaborated FETD algorithm and to validate its reliability, the wideband finite difference time domain (FDTD) algorithm is applied. In the FDTD algorithm a uniform coboidal grid is used, and the maximum size of the Yee cell is determined using formula

$$\Delta_{x,\mathrm{FDTD}} \le \frac{1}{10}\cdot \min\left(v_m\right)\cdot f_{I,\max}^{-1} = \frac{1}{10}\cdot \min\left(\frac{c}{\sqrt{\mu_r\left(\varepsilon_\infty + \Delta_\varepsilon\right)}}\right)\cdot f_{I,\max}^{-1}, \tag{19}$$

where v_m is the velocity of electromagnetic wave in a material, and c is the velocity of the wave in the vacuum.

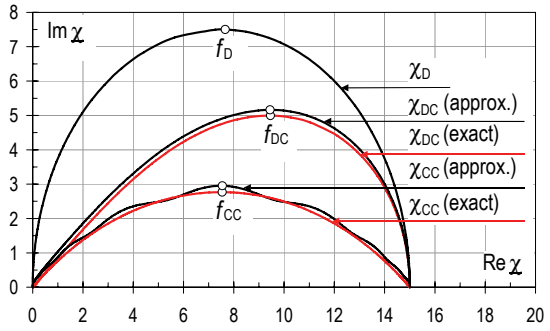

Fig. 5. Complex susceptibility of the initial and the approximated models

Comparison of the electromagnetic response calculated using the FETD and the FDTD algorithms are shown in Figs. 6-7. Both, the trend of the calculated waveforms, stated by the low frequency components, and the extreme values of the field, are similar. The presented graphs reveal inferiority of the finite difference approach. The FDTD waveforms are characterrized by some high-frequency fluctuations of the instantaneous values. The largest noticeable differences in the calculated field occur when the incident wave changes rapidly.

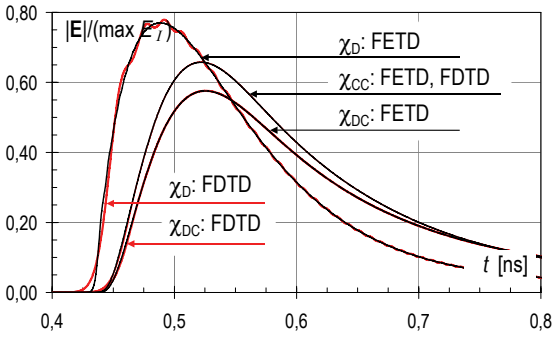

Fig. 6. Waveform response at the point P_1 (inside the plate)

These perceptible artifacts arise due to implementation of the simple linear differential approximations in space and in time. The presented results indicate, the FETD algorithm is better than the FDTD. The waveforms calculated using the FETD scheme are smoother. The finite element results are reasonable since the higher order approximation is used and the constructed mesh is locally adapted.

The computed amplitude spectrums confirm these findings (Fig. 8). Some perceptible differences between the FDTD and the FETD algorithm appear over 2 GHz, but the magnitudes of these harmonics are less than 0.08.

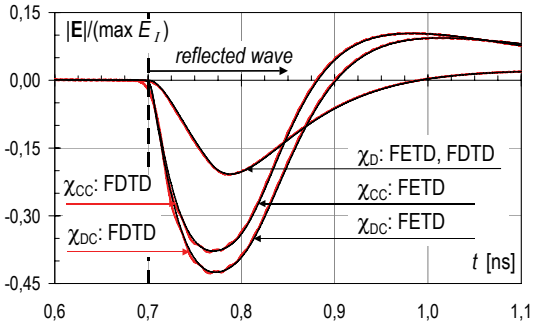

Fig. 7. Reflected wave registered at the point P_2 (in front of the plate)

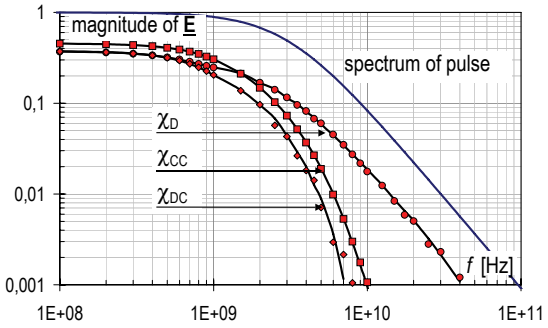

Fig. 8. Amplitude spectrum of electric field intensity at point P_1 (FDTD: results denote by tags, FETD: the curves)

To quantify differences between calculated waveforms, a relative measure of the error is introduced

$$\delta_E = \frac{\max\left|\left|\vec{\boldsymbol{E}}_{\mathrm{FDTD}}\left(n\Delta_t\right)\right| - \left|\vec{\boldsymbol{E}}_{\mathrm{FETD}}\left(n\Delta_t\right)\right|\right|}{\max\left|\vec{\boldsymbol{E}}_{\mathrm{FDTD}}\left(n\Delta_t\right)\right|} \cdot 100\% \,, \tag{20}$$

where the maximum value of the field obtained from the FDTD algorithm is the reference value. Figs. 9 and 10 show the relation between the maximum value of the computational error and the time integration step. For completeness, depicting plots are correlated with the relaxation time distribution function f_τ, and the components $\chi_{\mathrm{D},k}$ of the approximated model. Much closer agreement between results is noticed for the smallest time step Δ_t. In this case the maximum value of the error δ_E does not increase 1.3%. Extensive numerical tests indicate that the maximum value of the error becomes larger when the time integration step Δ_t increases. The maximum value of the error does not exceed 17.4% when value of the time integration step and the relaxation time of the first pole $\chi_{\mathrm{D},1}$ are comparable. The observed trend arises from a relatively small value of the permittivity decrement $\Delta_{\varepsilon,k}$ of the early components $\{\chi_{\mathrm{D},1}, \chi_{\mathrm{D},2}, \ldots\}$ of the approximated model (Table 1).

To reduce the error of computations the size of the finite elements and the value of the time integration step should be decreased. Unfortunately, in this case the efficiency of the FETD algorithm is slipped down. It is the implicit scheme, while the wideband formulation of the finite difference algorithm remains explicit [10]. The FDTD algorithm is faster, but the Courant condition must be fulfill to assure the stability of the algorithm.

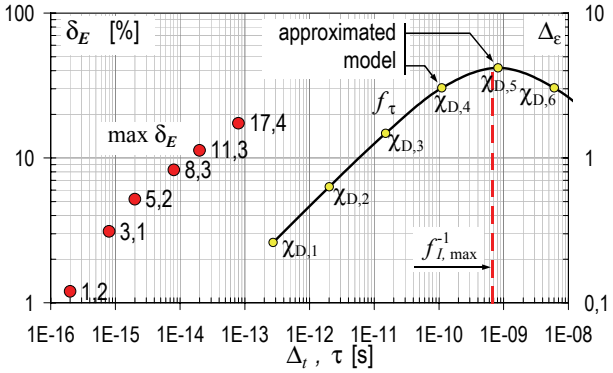

Fig. 9. Correlation between the error δ_E and the time integration step Δ_t for the Cole-Cole model

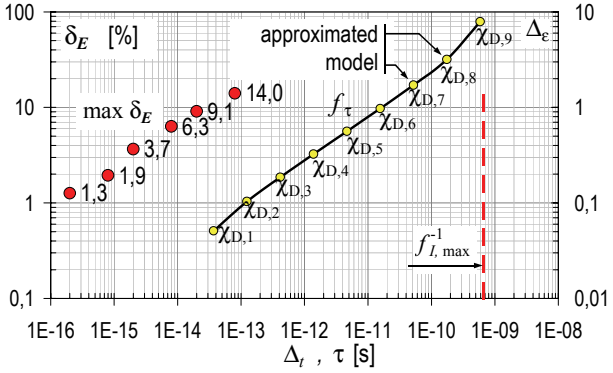

Fig. 10. Dependence of the error δ_E on the time integration step Δ_t for the Davidson-Cole model

5. Terms of realization

The elaborated tests enable to determine some essential constraints of the wideband FETD scheme. The set of restrictions connected with the broadband analysis is broader than the constraints defined for the narrowband problems. The narrowband formulation provides only some coarse, preliminary restrictions. Fig. 11 summarizes the factors that should be taken into consideration.

The form of the approximated model of susceptibility $\{\chi_{D,1}, \chi_{D,2}, \ldots, \chi_{D,Nm}\}$ is the principal factor determining the properties of the broadband algorithm. Since the number of poles N_m is limited, the spectrum of the relaxation phenomena, particularly for fractional models, is reduced. To minimise the error of analysis, the constructed model (4) should be as near as possible to the empirical form. The definition of the approximated model requires to choose the number of sub-models, and to determine the parameters describing their dynamics.

Further restrictions related to the wideband scheme arise from geometry and material structure of the model. The distinguished conditions have an effect on the construction of the FE mesh, and the value of the time integration step.

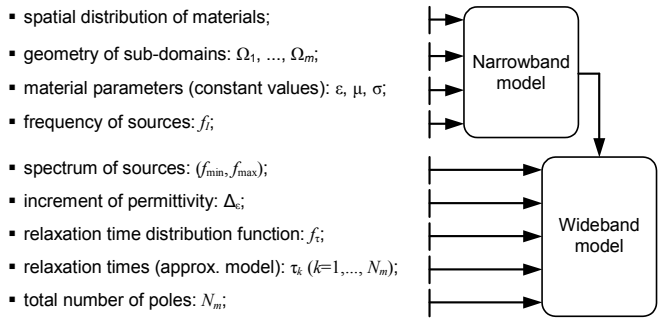

Fig. 11. List of factors determining the form of the wideband algorithm

The size of inscribed FE mesh depends on the local wavelength of EM wave. As a result of shortening the length of the electromagnetic wave, the FE grid must be locally adapted. The largest, acceptable linear size of the element implicitly comes from the value of permittivity (cf. Eq. (15))

$$\Delta_{\mathrm{FE}} \propto \min \frac{v_m}{f_{I,\max}}. \tag{21}$$

The value of time integration step Δ_t is linked to the dynamics of assumed model of susceptibility and the bandwidth of the propagated waveform.

$$\Delta_t << \left\{ f_{I,\max}^{-1}, \tau_1, \tau_2, \ldots, \tau_{N_m} \right\}. \tag{22}$$

The given examples indicate that the accepted time step Δ_t should be at least hundredfold smaller than the time parameters describing the dynamics of polarization phenomena.

6. Conclusions

In the paper the wideband formulation of the finite element time domain algorithm is presented. The discussed scheme can be implemented to the broadband analysis of electromagnetic phenomena in some components containing dispersive materials. The proposed method can potentially be applied to modeling some linear media, with homogenized structure. Various fractional relaxation model of permittivity can be used as inputs to prepare the realistic description of the analyzed phenomena.

The structure of the presented FETD algorithm is flexible. The numerical routines applied to the narrowband part and the supplementary part can be independently selected. Since the fractional models of susceptibility require a greater number of components of the approximated series, the number of sub-models in the dispersive part is not limited within the algorithm. The number of poles N_m is only bounded by the size of available memory of the computer.

It should be stressed, the supplementary part of the FETD algorithm can take a multimodal form. The convolution integrals can be computed using different schemes, because the order

of the approximated polynomial $\boldsymbol{e}_{\Delta}$ can be adjusted to the relation between the relaxation time τ_k and the time integration step Δ_t.

The conducted numerical tests reveal some properties of the wideband finite element scheme and its relation to the finite difference algorithm [6]. Considering the basic metrics of numerical performance, the FDTD scheme has the clear advantage. Its computational time is considerably shorter since the wideband FDTD algorithm is explicit. Unfortunately, the structured and uniform differential mesh is not convenient in the broadband analysis. The regular FD mesh has to be adjusted to some regions of interests (ROI's) where the frequency dependent permittivity reaches the largest value. The resultant mesh is oversized, but some details of geometry and curved surfaces have to be simplified. The comparative analysis shows the rationality and better properties of the finite element approach. The form of the FE wideband model can be adjusted to the complex geometry and local values of permittivity. The FE full-wave time-domain simulator is more time-consuming, but both the structure of the wideband algorithm and the implemented routines can be modified.

Acknowledgements
This work was prepared under scientific work S/WE/1/13 and supported by the Polish Ministry of Science and Higher Education.

References

[1] Lee W.-J., Kim C.-G., *Electromagnetic wave absorbing composites with a square patterned conducting polymer layer for wide band characteristics*, Shock and Vibration, no. 1, pp. 1-5 (2014).
[2] Taya M., *Electronic composites*, Cambridge University Press (2005).
[3] Fourn C., Lasquellec S., Brosseau C., *Finite-element modeling method for the study of dielectric relaxation at high frequencies of heterostructures made of multilayered particle*, Journal of Applied Physics, vol. 102, no. 12, pp. 124107-11 (2007).
[4] Kalmykov Y.P., Coffey W.T., Crothers D.S.F., Titov S.V., *Microscopic models for dielectric relaxation in disordered systems*, Physics Review, serie E, vol. 70, no. 4, pp. 041-103 (2004).
[5] Raju G.G., *Dielectrics in electric fields*, CRC Press (2003).
[6] Butryło B., *Parallel computations of electromagnetic fields in models with dispersive materials* (in Polish), Bialystok University of Technology (2012).
[7] Charef A., *Modeling and analog realization of the fundamental linear fractional order differential equation*, Nonlinear Dynamics, vol. 46, pp. 195-210 (2006).
[8] Rao S.M., *Time domain electromagnetics*. Academic Press (1999).
[9] Oughstun K.E., *Electromagnetic and optical pulse propagation*, Springer (2006).
[10] Young J.L., Nelson R.O., *A summary and systematic analysis of FDTD algorithms for linearly dispersive media*, IEEE Antennas and Propagation Magazine, vol. 43, no. 1, pp. 61-77 (2001).
[11] Ramadan O., *Unconditionally stable split-step finite difference time domain formulations for double-dispersive electromagnetic materials*, Computer Physics Communications, vol. 185, no. 12, pp. 3094-3098 (2014).
[12] Causley M.F., Petropoulos P.G., *On the time-domain response of Havriliak-Negami dielectrics*, IEEE Transactions on Antennas and Propagation, vol. 61, no. 6, pp. 3182-3189 (2013).
[13] Maradei F., *A frequency-dependent WETD formulation for dispersive materials*, IEEE Transactions on Magnetics, vol. 37, no. 5, pp. 3303-3306 (2001).
[14] Stoykov N.S., Kuiken T.A., Lowery M.M., Taflove A., *Finite-element time-domain algorithms for modeling linear Debye and Lorentz dielectric dispersions at low frequencies*, IEEE Transactions on Biomedical Engineering, vol. 50, no. 9, pp. 1100-1107 (2003).
[15] Monk P., *Finite element methods for Maxwell's equations*, Oxford University Press (2003).